ORIGINAL ARTICLE

O_2 permeability of lipid bilayers is low, but increases with membrane cholesterol

Samer Al-Samir[1] · Fabian Itel[2] · Jan Hegermann[3] · Gerolf Gros[1] · Georgios Tsiavaliaris[4] · Volker Endeward[1]

Abstract

Oxygen on its transport route from lung to tissue mitochondria has to cross several cell membranes. The permeability value of membranes for O_2 (P_{O2}), although of fundamental importance, is controversial. Previous studies by mostly indirect methods diverge between 0.6 and 125 cm/s. Here, we use a most direct approach by observing transmembrane O_2 fluxes out of 100 nm liposomes at defined transmembrane O_2 gradients in a stopped-flow system. Due to the small size of the liposomes intra- as well as extraliposomal diffusion processes do not affect the overall kinetics of the O_2 release process. We find, for cholesterol-free liposomes, the unexpectedly low P_{O2} value of 0.03 cm/s at 35 °C. This P_{O2} would present a serious obstacle to O_2 entering or leaving the erythrocyte. Cholesterol turns out to be a novel major modifier of P_{O2}, able to increase P_{O2} by an order of magnitude. With a membrane cholesterol of 45 mol% as it occurs in erythrocytes, P_{O2} rises to 0.2 cm/s at 35 °C. This P_{O2} is just sufficient to ensure complete O_2 loading during passage of erythrocytes through the lung's capillary bed under the conditions of rest as well as maximal exercise.

Keywords Hemoglobin deoxygenation · Hemoglobin-loaded liposomes · O_2 net flux across membranes · Stopped-flow technique · Deoxygenation by mixing with dithionite

Introduction

It has long been thought that the respiratory gases permeate all cell membranes without noticeable resistance. In recent years, however, this assumption has been rebutted by several studies, at least for carbon dioxide, for which it has been shown that membranes can present a significant diffusion resistance that drastically rises with higher cholesterol levels in the membrane [1–6], and on the other hand, can be greatly alleviated by the incorporation of protein gas channels such as aquaporin-1 or Rhesus-associated glycoprotein [2, 7–10]. In the case of the permeation of oxygen across membranes, current data mainly obtained from ESR spin label studies [11], or other indirect biophysical techniques such as fluorescence quenching and molecular dynamics (MD) simulations [12–14] have reported for liposomes extremely high permeabilities of 20–125 cm/s that would physiologically amount to zero resistance in the case of a cell membrane. O_2 permeabilities between 10 and 100 cm/s are shown at the end of this paper to exert no detectable influence on the deoxygenation kinetics of red cells. Thus, such P_{O2} values have no influence on the overall deoxygenation process, whose kinetics then is determined by the hemoglobin deoxygenation kinetics and by intracellular diffusion only.

So far, no O_2 permeabilities of liposomes have been determined from direct measurements of O_2 flux across the liposome membrane. The only reasonably sensitive P_{O2} determination based on an O_2 flux observed across a cell membrane to our knowledge is that of Holland et al. [15], who report an orders of magnitude lower P_{O2}

Georgios Tsiavaliaris and Volker Endeward contributed equally to this work.

✉ Gerolf Gros
Gros.Gerolf@MH-Hannover.de

1 AG Vegetative Physiologie 4220, Zentrum Physiologie, Medizinische Hochschule Hannover, 30625 Hannover, Germany

2 Empa, Swiss Federal Laboratories for Materials Science and Technology, Lerchenfeldstr. 5, CH-9014 St. Gallen, Switzerland

3 Abteilung Funktionelle und Angewandte Anatomie, Elektronenmikroskopie 8840, Medizinische Hochschule Hannover, 30625 Hannover, Germany

4 Abteilung Biophysikalische Chemie 4350, Medizinische Hochschule Hannover, 30625 Hannover, Germany

value of 0.6–0.8 cm/s for the red cell membrane using the stopped-flow technique. This discrepancy prompted us to readdress the question of membrane permeability to O_2, following the strategy of using—instead of cells— the much simpler model of unilamellar lipid vesicles of 50 nm radius loaded with oxyhemoglobin. We measured the efflux of O_2 across the lipid membrane of this artificial but easily modifiable system. This was achieved by mixing the suspension of oxyhemoglobin-loaded liposomes in a rapid reaction stopped-flow apparatus with a 50 mM dithionite solution that within 1 ms consumes dissolved O_2 in the extraliposomal space, and thus practically instantaneously after mixing has established a zero partial pressure of O_2 in this space. The O_2 diffusing out of the liposome after dissociation from hemoglobin was quantitated by spectrophotometry of the intraliposomal hemoglobin at a suitable wavelength and followed over time. The time course of the observed transients represents the deoxygenation kinetics of the intraliposomal oxyhemoglobin. To derive the P_{O2} of the liposome membrane, we compared this kinetics with that of pure hemoglobin solution. We prepared liposomes from the most common lipids found in mammalian cell membranes, namely phosphatidylcholine (PC), phosphatidylethanolamine (PE) at a ratio of 8:2 (moles/mole) and different cholesterol (Chol) concentrations ranging from 0 up to 70 mol%.

The major physiological message from this study is that phospholipid membranes containing cholesterol in a concentration equalling that of the erythrocyte membrane (45 mol%), possess a P_{O2} not far in excess of physiological requirements but well adapted to physiological needs, and just sufficient to allow complete blood oxygenation in the lung at rest as well as at maximal aerobic exercise.

Results

Properties of liposomes

Here, we studied aspects of the liposomes that are important for the interpretation of the observed O_2 effluxes in terms of liposomal membrane O_2 permeability: are the liposomes unilamellar or multilamellar? What is the size and size distribution of the liposomes? How well are higher amounts of cholesterol incorporated into the membrane? Fig. 1 shows electron micrographs of liposomes with cholesterol contents of 0 and 50 mol%. It is apparent that for both types of vesicles the diameters are around 100 nm. In the presence of cholesterol the liposomes are entirely unilamellar, only in the complete absence of cholesterol a minor fraction has two membranes, an outer and an inner one. This fraction was quantified as constituting 12%. To quantitate the size of the liposomes, we used dynamic light scattering, DLS, providing the intensity size distributions exemplified in Fig. 2. Figure 2a and b show both narrow size distributions with average radii of the liposomes of about 50 nm [a: 51.1 ± 11 (SD) nm, b: 50.2 ± 8.2 (SD) nm]. This radius was found with minor variations (50–57 nm) in all the preparations used here. Figure 2 shows that contamination by lower size particles was very minor. A radius of 50 nm is in excellent agreement with the liposome diameter of around 100 nm as apparent in the electron micrographs of Fig. 1. To validate the incorporation of cholesterol into the lipid bilayer, we experimentally quantified the cholesterol and phosphatidylcholine content of the liposomes. Between 0 and 50 mol% cholesterol, the experimental ratios of cholesterol/phosphatidylcholine closely follow the "theoretical" values as they are present in the initial lipid mixture from which the liposomes are generated. Only at cholesterol concentrations above 50 mol% the experimental ratios are somewhat lower than the theoretical ratios. This suggests that

Fig. 1 Transmission electron micrographs of liposomes containing 0 (**a**) and 50 mol% cholesterol (**b**) in their membrane
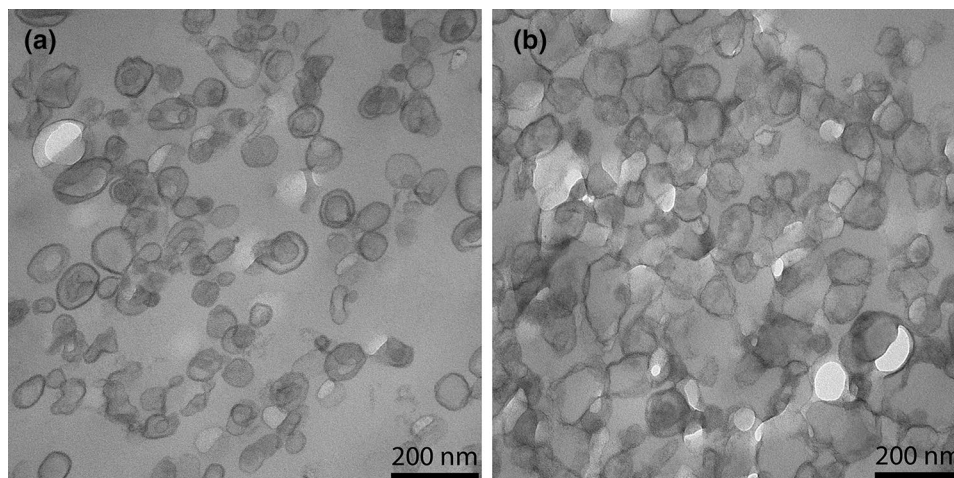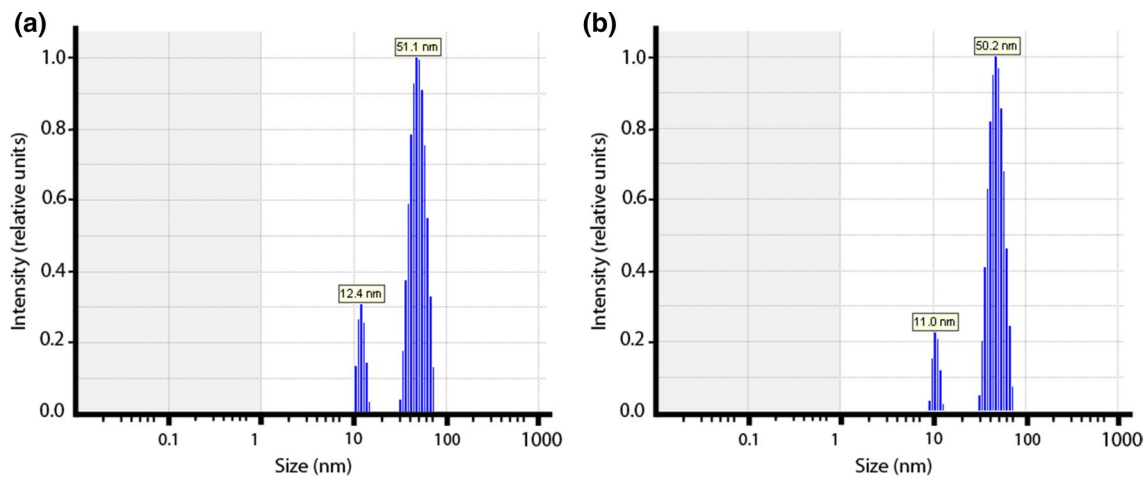
Fig. 2 Vesicle size distributions by dynamic light scattering. **a** Liposomes without membrane cholesterol exhibit an average radius of 51.1 nm, **b** liposomes with 50 mol% cholesterol an average radius of 50.2 nm. All liposome preparations gave similar distributions with radii of around 50 nm. There were only minor contaminations with particles of a radius around 10 nm

cholesterol incorporation up to 50 mol% is proportional to the cholesterol concentration present in the lipid mixture, while above 50 mol% cholesterol incorporation into the lipid bilayer begins to become limited. It should be noted that in the results given below, we always use the cholesterol fractions expected from the lipid composition employed for preparation (theoretical value).

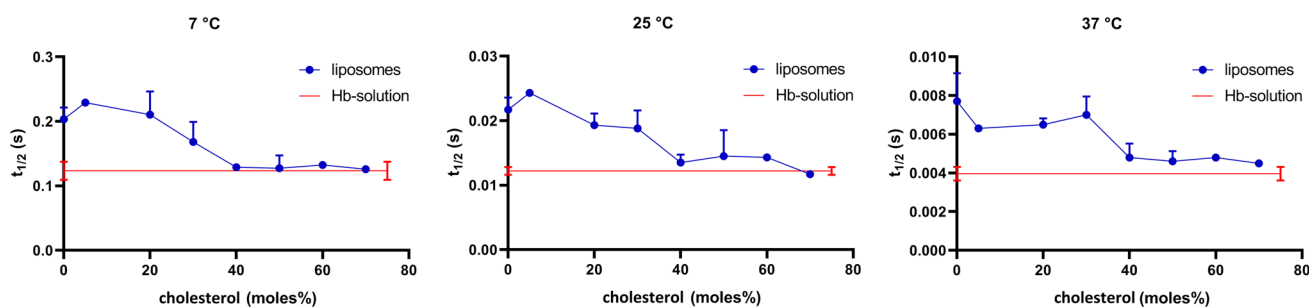## Kinetics of the deoxygenation of oxyhemoglobin-loaded liposomes

Here, we present the results of stopped-flow experiments measuring the kinetics of hemoglobin deoxygenation and O$_2$ efflux from liposomes. Figure 3 shows original stopped-flow tracings at the three temperatures studied for pure hemoglobin solution, and for suspensions of liposomes loaded

with oxyhemoglobin with 0 and 40 mol% membrane cholesterol (other cholesterol concentrations not shown). All the liposomes possess a slower kinetics than hemoglobin solution. However, the difference is greatest for the liposomes lacking cholesterol in their membrane, and smallest for the liposomes having 40 mol% cholesterol. Thus, it appears that the presence of a membrane between the hemoglobin and the dithionite slows down the deoxygenation process to an extent dependent on membrane cholesterol. The kinetics of the original stopped-flow tracings are quantified in terms of half-times in Fig. 4, which shows the results for all liposomal cholesterol concentrations studied. The curves confirm that liposomes with 0% cholesterol exhibit the slowest kinetics, while with 40% cholesterol an almost twice as fast kinetics is observed, and the half-times approach the values of the hemoglobin solutions. The results of Fig. 4 can
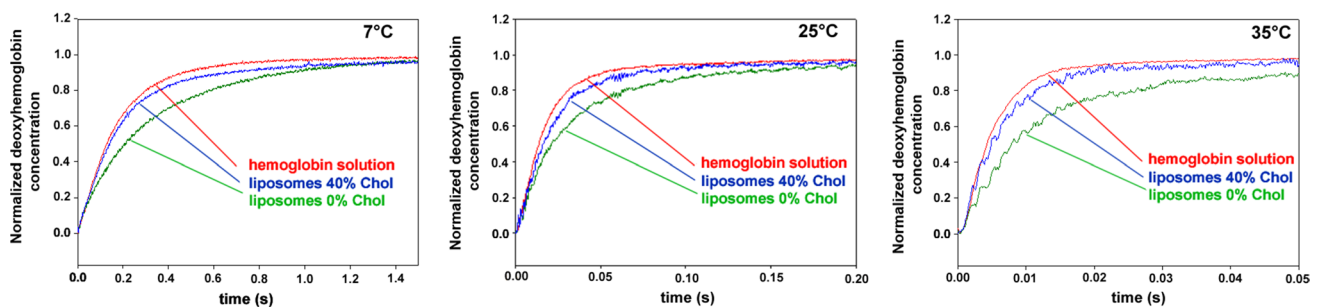
Fig. 3 Original records of stopped-flow experiments with hemoglobin solutions and liposome suspensions. *Y*-axis: the normalized relative change of absorbance at 436 nm (liposomes) or 470 nm (hemoglobin solutions), respectively. The records show the disappearance of oxyhemoglobin after mixing with dithionite solution. Red (and uppermost) curves hemoglobin solution, blue (and middle) curves liposomes with 40 mol% cholesterol, green (and lowermost) curves liposomes with 0% cholesterol. At the three temperatures 7 °, 25 ° and 35 °C, the kinetics of all liposomes is slower than that of hemoglobin solution, the liposomes with 0 mol% cholesterol exhibiting the slowest kinetics. All records represent the averages of 8 single stopped-flow shots. Normalization of the *Y*-axis was done by subtracting the starting absorbance value from the curve and setting the amplitude of the signal to 1.0

Fig. 4 Half-times $t_{1/2}$ of the stopped-flow deoxygenation kinetics of hemoglobin-loaded liposomes and pure hemoglobin solutions. Membrane cholesterol clearly reduces the difference between liposomes and pure hemoglobin solutions. At all temperatures, most of this effect occurs between 20 or 30 and 40 mol% cholesterol. Each point represents between 2 and 4 experimental stopped-flow series, each series comprising 8 single stopped-flow shots. n for hemoglobin solutions was ≥ 8. Bars represent S.D. values where applicable

be summarized in three points: (1) between a membrane cholesterol of 0 and 20 mol%, the half-times of the deoxygenation kinetics are rather similar to each other and are all about $2 \times$ greater than those of pure hemoglobin; (2) between membrane cholesterol concentrations of 40 and 70 mol%, half-times are also quite similar at a considerably lower level, being only slightly above those of pure hemoglobin solution; (3) between 30 and 40 mol% cholesterol, a step seems to occur in all curves that is associated with a drastic decrease in half-times. This suggests that between 30 and 40% the slowing influence of the membrane on $t_{1/2}$ diminishes greatly.

Figure 5 shows that the low-cholesterol $t_{1/2}$ values are highly statistically significantly different from the $t_{1/2}$ values for hemoglobin solution ($p < 0.0001$ at all temperatures).

"Low-cholesterol" was defined here as all $t_{1/2}$ values between 0 and 20 mol% cholesterol, a combination, which seems justified in view of the fact that there are only minor differences within this group. "High cholesterol" was defined as all values between 40 and 60 mol%, which again show hardly any differences within themselves. As "high-cholesterol" is fairly close to the hemoglobin values, it is not surprising that the difference between these two groups is not statistically significant ($p = 0.84$, 0.12, 0.096 at 7, 25 and 35 °C, respectively).

The temperature dependence of the kinetics of deoxygenation is illustrated in the Arrhenius plot shown in Fig. 6. The Y-axis represents the apparent dissociation constant k_d and was derived from the experimental $t_{1/2}$ of Fig. 4 as $k_d = \ln 2 / t_{1/2}$. The slope in Fig. 6 is about identical for hemoglobin
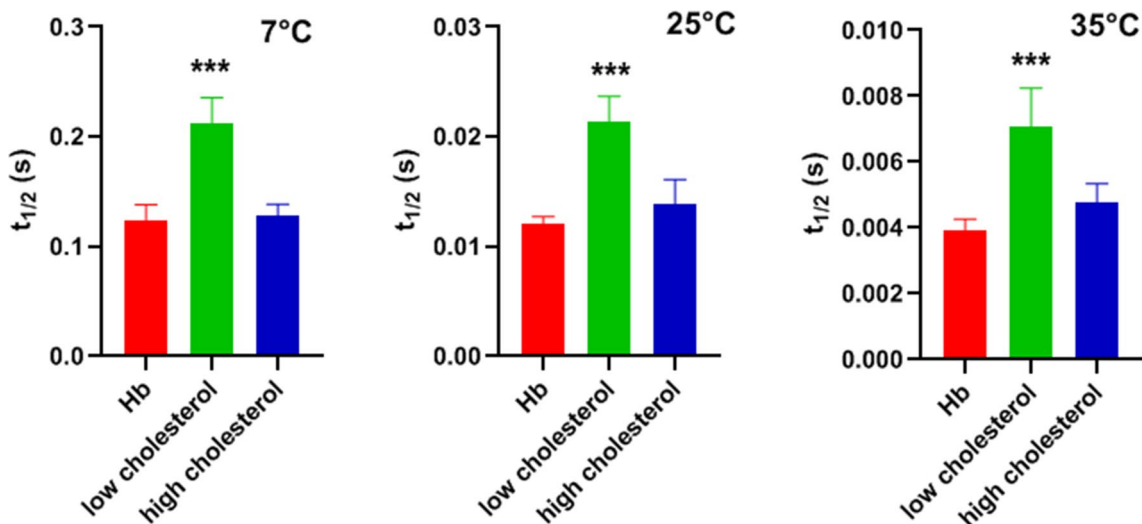
Fig. 5 Half-times for hemoglobin solutions, Hb, and low- and high-cholesterol liposomes, respectively. "Low cholesterol" represents all data of Fig. 4 between 0 and 20 mol% cholesterol, "high cholesterol" comprises the data of Fig. 4 for 40–60 mol%. One-Way ANOVA with Tukey post-test shows that low cholesterol $t_{1/2}$ is significantly greater than hemoglobin $t_{1/2}$ at all temperatures. "High cholesterol" data are also somewhat greater than hemoglobin $t_{1/2}$, but the difference does not reach statistical significance. Number of $t_{1/2}$ values per column is 9 for Hb, 6 for low cholesterol, and 6 for high cholesterol. ***Indicates $p < 0.0001$
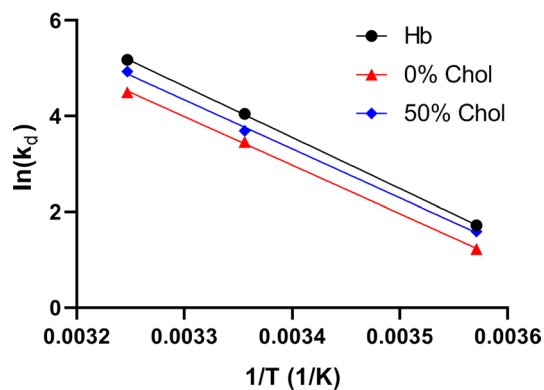
Fig. 6 Arrhenius plot describing the temperature dependence of the dissociation kinetics of O$_2$ from hemoglobin, in solution and within liposomes. k_d represents the apparent experimental dissociation reaction constant of HbO$_2$ (T is temperature in Kelvin). The activation energy Ea for all three solutions/suspensions is calculated to be 90 kJ/mol

solution, 0% Chol liposomes and 50% Chol liposomes. Thus, the activation energy is about 90 kJ/mol for all three systems. This is in fair agreement with activation energies previously reported for the oxyhemoglobin dissociation reaction [16]. This illustrates that the activation energy of the chemical reaction dominates also the combined reaction–diffusion process in liposomes. The intercept on the Y-axis represents ln (A), where A is the pre-exponential factor of the Arrhenius equation. ln (A) in Fig. 6 decreases in a systematic fashion with increasing diffusion resistance of the liposome membrane.
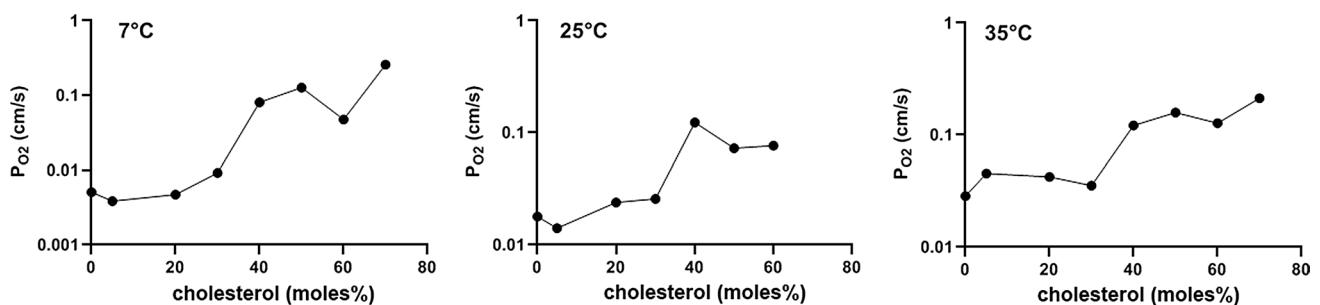
Oxygen permeability of liposomes

On the basis of the theory of O$_2$ release by liposomes described in "Methods", we have derived P$_{O2}$ values (Fig. 7) from the experimental t$_{1/2}$ values given in Fig. 4. The O$_2$ permeabilities in the absence of cholesterol are 0.0051 cm/s, 0.018 cm/s, and 0.029 cm/s for 7 °, 25 ° and 35 °C, respectively. This corresponds to a temperature dependence of

P$_{O2}$ at 0% cholesterol of 6.5%/°C, whereas O$_2$ diffusion in water exhibits a temperature dependence of about 3%/°C [17]. Figure 7 also shows the dependencies of P$_{O2}$ on membrane cholesterol for the three temperatures. As already apparent in Figs. 3 and 4, the resistance of the membrane for O$_2$ decreases, and its permeability increases, when the cholesterol fraction in the membrane is raised. This holds equally for all temperatures studied. However, between 0 and 20 mol% cholesterol, there is little effect of cholesterol on P$_{O2}$. This implies that "low cholesterol" membranes (0–20%) exhibit the highest resistance toward the transfer of O$_2$. Only when cholesterol increases from 30 to 70% ("high cholesterol"), there is a clear increase in permeability and thus a decrease of O$_2$ diffusion resistance. This increase in P$_{O2}$ amounts to about a factor of 10 between 0 and 70 mol% (a little less for the 60 mol% at 25 °C). It is noteworthy that for all temperatures measured the most pronounced increase in P$_{O2}$ occurs between 30 and 40 mol% cholesterol. At 50% cholesterol and above, the kinetics of Hb-loaded liposomes approach quite closely the kinetics of the pure hemoglobin solution (Fig. 4). Interestingly, at these cholesterol fractions, the temperature dependence of P$_{O2}$ is small or absent (Fig. 7).

Discussion

Limitations of the present experimental approach and comparison with the other approaches

The present stopped-flow technique derives O$_2$ membrane permeability from the transmembrane O$_2$ concentration gradient and from the flux of O$_2$ across the liposome membrane. While the extraliposomal O$_2$ partial pressure (pO$_2$) is always nearly zero due to the presence of dithionite (see explanations in "Methods", section "Stopped-flow experiments"), the intraliposomal pO$_2$ and the efflux of O$_2$ can be derived from the changes in intraliposomal oxygen saturation of hemoglobin, which is the major measured parameter.

Fig. 7 Oxygen permeabilities of liposomes at 7, 25 and 35 °C. All permeabilities are lowest in the absence of cholesterol, and increase by about one order of magnitude with increasing cholesterol content in the membrane

Knowledge of the thickness of the membrane is not directly necessary for determining membrane P_{O_2}, but as is apparent from Eqs. 3 and 4 given in the "Methods" section, *Theory*, knowledge of the surface-to-volume ratio a/v is required and this quantity is affected by the assumed thickness of the membrane. a and v are obtained from the experimentally determined diameter of the liposomes (Fig. 2), assuming a spherical geometry, which is roughly in accordance with the appearance of the liposomes in transmission electron microscopic images (Fig. 1). In conjunction with this, we assume a membrane thickness of 5 nm. Two alternative approaches to calculate P_{O_2} from the experimental half-times of the stopped-flow records are employed, as discussed in "Methods", Theory, after Eq. 4 and after Eq. 6. The resulting uncertainty in $t_{1/2}$ of the calculated deoxygenation kinetics, however, is shown there not to exceed 3%, which we consider to be of minor importance.

A major limitation of the present method is the lack of information provided on the intra-membrane inhomogeneity. We must treat the membrane as a "black box" and determine only its overall permeability. However, it has been shown in much detail, e.g. by molecular dynamics simulations, that the lipid bilayer is highly inhomogeneous with respect to free energy, O_2 solubility and diffusivity [12, 13, 18, 19]. Our data shed no light on these intra-membrane properties.

As discussed in detail below, the present results are greatly at variance with P_{O_2} values of lipid bilayers reported from several ESR measurements [11] and MD simulations [12, 13, 18–20] by one to four orders of magnitude. In addition, we find that membrane cholesterol increases P_{O_2}, whereas with ESR [11] and MD simulations [20, 21], a moderate decrease in P_{O_2} is observed. While our data provide no molecular explanation for these discrepancies, it is obvious that there is a fundamental difference between the present and the two other mentioned techniques: in MD calculations as well as in ESR, O_2 and the membrane are in equilibrium and no net flux of O_2 occurs. In the stopped-flow approach, an initial O_2 gradient is set up and we follow its decay, from whose kinetics we determine P_{O_2}. Possibly, this is the key to the discrepancy, although the responsible mechanism is not understood as yet. It should be noted, however, that the present approach simulates the in vivo situation, where O_2 gradients drive the net uptake of O_2 from the lung into the blood as well as the net release of O_2 from the blood to the O_2-consuming tissues.

Role of unstirred layers and multilamellar liposomes

The effect of unstirred layers on permeability measurements across lipid membranes have often led to controversial discussions. Therefore, we will discuss here the role of unstirred layers in the present experimental approach. The P_{O_2} values calculated from the stopped-flow records could

in principle be underestimated by the presence of unstirred layers on the external surface of the liposomes and by intraliposomal unstirred layers. We believe that unstirred layers in the present measurements do not affect P_{O_2} for the following reasons:

1) The present vesicles are so small that extravesicular unstirred water layer thicknesses constitute no significant diffusion resistance [22, 23]. From the hydrodynamic treatment of Landau and Lifschitz [24] (p. 224), it follows that under conditions of turbulent flow, as it occurs in the mixing chamber of the stopped-flow apparatus, the thickness of the unstirred boundary layer δ is proportional to the length of the object ℓ, if all other conditions are identical. In stopped-flow experiments analogous to ours with human red cells at 37 °C, an unstirred layer thickness of 0.7 μm has been reported [15]. With ℓ = 8 μm for red cells and ℓ = 100 nm for the present liposomes, a δ for the present liposomes of 9 nm is predicted. The apparent permeability of such a water layer for O_2 would be $D_{O_2}/\delta = 3 \cdot 10^{-5}$ cm²/s/9 · 10^{-7} cm = 33 cm/s (where D_{O_2} is the diffusion coefficient of O_2 in water [17]). This O_2 permeability of the unstirred layer is at least two orders of magnitude greater than the permeabilities of Fig. 7. Thus, it can have no effect of the calculated P_{O_2}. A further, and equally striking, argument against a role of an extravesicular unstirred layer is the high concentration of dithionite (50 mM) in the solution with which the liposome suspensions are mixed in the stopped-flow apparatus. As the consumption of O_2 by dithionite occurs at an about equimolar ratio, we have a huge O_2 uptake capacity in the extravesicular space, orders of magnitude greater than the O_2 present in the system. Due to the high speed of this reaction, this will the ensure that all O_2 leaving the liposome will be consumed practically immediately by dithionite [as explained in "Methods" ("Stopped-flow experiments")], even if there existed a poorly stirred zone on the liposome surface. Such a poorly stirred layer will acquire the dithionite concentration of the surrounding solution by diffusion within < 1 ms, the dead time of the stopped-flow instrument: assuming a diffusion coefficient of 10^{-6} cm²/s for dithionite and using Crank's equations and graphical solution ([25], pp. 14–15, Fig. 2.3) one calculates that within 1 ms an unstirred layer even of 500 nm thickness will have assumed the dithionite concentration of the surrounding solution simply by diffusion without any convection. In addition, it may be noted that an only 9-nm-thick layer around the liposome with a dithionite concentration of 50 mM can absorb 3 times as much oxygen as is initially present inside the liposome. We conclude that due to both, the presence of dithionite and the marginal thickness of the unstirred layers, extravesicular unstirred layers cannot affect the experimental P_{O_2} in the present experiments.

2) An alternative factor reducing the apparent P_{O_2} could be an intravesicular unstirred layer, meaning that

intravesicular diffusion processes would slow down the process of O_2 release by the liposomes. To study this, we have simulated the process of O_2 release ignoring or taking into account the intravesicular diffusion processes of O_2 and hemoglobin with the equation systems described in "Methods", "Theory of O_2 release by liposomes and calculation of O_2 permeabilities". We compare there a theoretical model assuming a stirred intravesicular volume with one that takes into account intravesicular diffusion processes. Half-times of the deoxygenation kinetics differ between these models by < 1% for a broad range of P_{O2} values.

Thus, in all the cases and over the entire range of possible P_{O2} values, the intravesicular diffusion has no effect on the half-time of the kinetics of O_2 release, because the diffusion times inside the small vesicles are extremely short. This conclusion holds for all the temperatures used in this study. An additional calculation shows that with $P_{O2} = 0.1$ cm/s, the influence of intravesicular diffusion becomes detectable at vesicle radii >> 100 nm only. Thus, with the present vesicle radii of 50 nm, intravesicular diffusion, or the intravesicular "unstirred layer", does not influence the estimated P_{O2} values. In conclusion, the present measurements are affected neither by extravesicular nor by intravesicular unstirred layer effects.

3) As discussed in conjunction with the electron micrographs of Fig. 1, only 12% of the liposomes without cholesterol are more than unilamellar, usually with a second membrane within the primary liposome. In contrast, all cholesterol-containing liposomes are purely unilamellar. To which extent can the presence of a second membrane on the inside of the outer membrane affect the measured O_2 permeability? Ignoring the surface areas and assuming identical properties of outer and inner membranes, the diffusion resistance of the "bilamellar" liposomes is given by $2/P_{O2}$, while that of the unilamellar vesicle is $1/P_{O2}$. Considering uni- and bilamellar liposomes as parallel resistances towards O_2, we obtain an overall inverse resistance of $1/R_{total} = 0.12 \cdot P_{O2}/2 + 0.88 \cdot P_{O2} = 0.94 \cdot P_{O2}$ cm/s. In other words, the presence of a small fraction of multilamellar liposomes affects the estimated P_{O2} by no more than 6%, i.e., the effect is almost negligible. Thus, the P_{O2}- concentration curves of Fig. 7 will remain practically unaltered.

Oxygen and carbon dioxide permeability in membranes

The present determinations of oxygen permeability, in contrast to earlier approaches, are based on direct measurements of O_2 flux across a phospholipid bilayer. At a cholesterol concentration of ~ 45% as it occurs in several cell membranes including red cells, we find a P_{O2} of about 0.2 cm/s at 35 °C (Fig. 7). As will be shown below, this permeability is sufficiently great to guarantee a complete O_2 equilibration

of the red cell interior under conditions of rest, and a 95% complete O_2 exchange even at the short capillary transit times in the lung as they may occur under heavy exercise [26]. Thus, this permeability is sufficient for pulmonary O_2 exchange, and likely also for O_2 release in most tissues, in which O_2 fluxes are not as great as they are required across the red cell membrane.

These results are remarkable in three important aspects that call for discussion:

1) The absolute value of P_{O2} determined here is much lower than has been derived from molecular dynamics simulations, which estimate P_{O2} values of 23 cm/s at 25 °C and 26–39 cm/s at 37 °C [12] or 20 cm/s at 25 °C [13]. This holds for the P_{O2} values of Fig. 7 with and without cholesterol. In addition, the present values are considerably lower than has been estimated from long-pulse saturation recovery ESR technique by the group of Subczynski [11], who report P_{O2} values of cholesterol-free phospholipid vesicles to be 125 cm/s at 29 °C. As discussed, unstirred layers on the external surface of the vesicles are not expected to play a role in our measurements and thus to reduce the apparent P_{O2}. We note that Holland and coworkers [15], using a direct O_2 flux measurement across the red cell membrane with a stopped-flow technique, after correction for an unstirred layer, obtained a P_{O2} of 0.6–0.8 cm/s for this membrane at 37 °C. This is in a range comparable to our value of 0.2 cm/s for liposomes containing 45% cholesterol.

Oxygen permeability of liposomes vs. CO_2 permeability: Figure 8 shows a comparison of the dependencies of P_{O2} and P_{CO2} of liposomes on membrane cholesterol. The former represent data from Fig. 7, the latter have been obtained by the mass spectrometric method applied to liposomes [2]. We note that these mass spectrometric results for P_{CO2} have qualitatively been confirmed
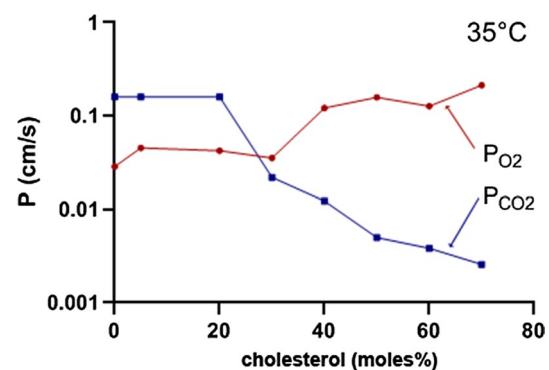

Fig. 8 Permeability of phospholipid vesicles for O_2 and CO_2 in dependence on membrane cholesterol. P_{O2} represents the data of Fig. 7, P_{CO2} is from the mass spectrometric measurements of Itel et al. [2]

by a stopped-flow technique [3]. While at the cholesterol concentration of the red cell membrane of 45% P_{O2} is 0.2 cm/s as just discussed, P_{CO2} is 0.008 cm/s, i.e., 25 times lower. Both curves refer to temperatures of 35 and 37 °C, respectively. This suggests a capability of membranes to become poorly permeable to CO_2 by incorporating high concentrations of cholesterol [2, 3], a property that is physiologically useful in some apical endothelial membranes [27–29]. On the other hand, in membranes possessing high cholesterol levels such as red cells, a required high permeability to CO_2 is achieved by the incorporation of protein CO_2 channels aquaporin-1 and Rhesus-associated glycoprotein, which results in a P_{CO2} of the human red cell membrane of ~ 0.15 cm/s [9, 10]. Figures 7 and 8 show that membrane cholesterol does not constitute a problem for O_2 transfer as P_{O2} is up to ten times higher than it is in the absence of cholesterol and also considerably higher than P_{CO2} above cholesterol concentrations of 30% (Fig. 8). We conclude that a membrane possessing a high cholesterol content in conjunction with protein CO_2 channels exhibits high permeabilities for CO_2 as well as for O_2, plus offers other advantages of high cholesterol such as a general barrier function as explained below and enhanced mechanical stability of the membrane.

2) It is well known that membrane cholesterol constitutes a drastic barrier towards uncharged hydrophilic molecules such as water and NH_3, but also formamide, acetamide, urea and glycerol [30], just as we show for CO_2 in Fig. 8. Oxygen, a small but relatively hydrophobic and lipophilic molecule (see, e.g., solubilities as compiled in [31]), differs radically from this behavior as shown in Figs. 7 and 8. P_{O2} increases with increasing membrane cholesterol. This is a novel finding that will favor O_2 transfer across high-cholesterol cell membranes, possibly without necessitating the presence of gas channels. As in the case of the absolute values of P_{O2} reported here, this finding is also in contrast to ESR-based measurements and molecular dynamics simulations. The ESR studies [11] predict a reduction of P_{O2} by 50% cholesterol to 1/5 of the value in the absence of cholesterol. Molecular dynamics simulations predict an only moderate reduction of O_2 permeability of phospholipid bilayers in the presence of cholesterol by 20% [20, 21, 32]. At present, there is no explanation for the discrepancy to the measurements of O_2 flux across the liposome membrane reported here. We note that increasing incorporation of the highly lipophilic cholesterol [33] into a phospholipid bilayer, besides condensing the membrane structure [34], will increase the amount of hydrophobic material present in the center of the membrane und may thus favor the passage of a small lipophilic molecules

like O_2 while increasing the hindrance to more hydrophilic molecules.

It is important to note that at all temperatures studied (Fig. 7), P_{O2} shows a step-like increase between 30 and 40 moles% cholesterol by almost one order of magnitude. This indicates that between these concentrations a major structural change occurs in the lipid bilayer that produces this tenfold increase in O_2 permeability. While the structural cause of this abrupt increase is not clear, it is known from studies of the elastic properties of phospholipid bilayers that between 30 and 50 moles% cholesterol in the membrane a similarly abrupt decrease in the critical area strain and in membrane toughness occurs [35]. This clearly indicates a major structural change in this concentration region associated with a decrease in cohesive energy density of the membrane-constituting material.

In conclusion, the present results indicate that the O_2 permeability of phospholipid membranes at high cholesterol, $P_{O2} = 0.2$ cm/s at 35 °C, are much lower than has previously been proposed. Second, P_{O2} depends inversely on membrane cholesterol compared to P_{CO2}: P_{O2} increases with increasing cholesterol by about one order of magnitude, while P_{CO2} decreases with increasing cholesterol by up to two orders of magnitude. At a lipid composition of the membrane similar to that of human red cells, P_{O2} is 25 times higher than P_{CO2}. This seems to make sense as a basic membrane property, as the gradients of dissolved O_2 between extra- and intracellular space, due to the 20 times lower solubility of O_2 compared to CO_2, are considerably smaller than those for CO_2.

Physiological significance of oxygen permeability and possible role of O_2 channels

What do the numbers for P_{O2} found here mean in terms of oxygen exchange in the body? We will study this question for the example of O_2 uptake by red cells in the lung. However, the answers will be similar for O_2 transport in the tissue. Figure 9 shows the kinetics of O_2 loading of red cells in the lung, calculated for different P_{O2} values of the red cell membrane. The equation system used is analogous to the one given in "Methods" for the release of O_2 from spherical liposomes and considers chemical reaction and diffusion processes of Hb and O_2 inside the red cell. However, the diffusion of O_2 from the alveolus into the red cell was treated as a one-dimensional diffusion process in deviation from the use of spherical coordinates for the liposomes. Due to the parachute-like deformation the red cell experiences in the lung capillary [36], we used as the intracellular diffusion path the total average thickness of the red cell of 1.6 μm and added to this a 1-μm-thick unstirred water layer representing the thickness of the alveolar-capillary barrier. The latter assumption supposes that the membranes within the
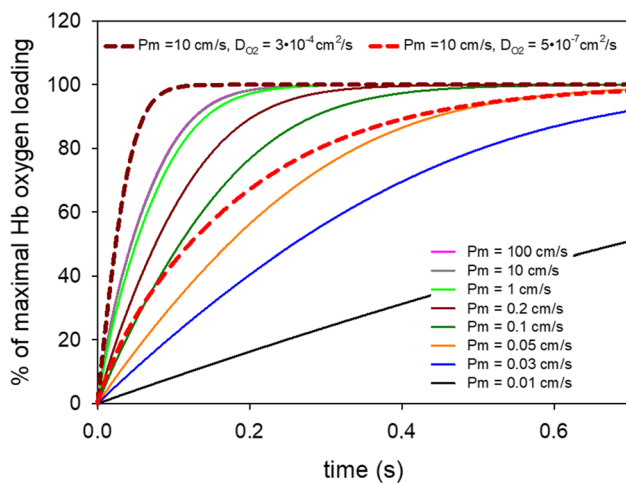
Fig. 9 Calculated time course of red cell oxygenation during passage through the lung capillary. The dashed curves are calculated for extremely high or extremely low intraerythrocytic O$_2$ diffusion coefficients together with an extremely high P$_{O2}$ (see numbers at the top of the figure). The solid curves are calculated with an intraerythrocytic O$_2$ diffusion coefficient of $0.8 \cdot 10^{-5}$ cm^2/s and a wide range of O$_2$ permeabilities from 0.01 to 100 cm/s. Note that the curves for 100 and 10 cm/s coincide completely (left-most continuous curve)

alveolar-capillary barrier constitute no significant diffusion barrier to O$_2$. Figure 9 shows the results of these calculations for the physiological temperature of 37 °C. The major results are as follows: P$_{O2}$ values of 100 and 10 cm/s coincide completely in the left-most continuous line, the line for P = 1 cm/s (bright green) deviates only very little from these two curves. In other words, physiologically it is irrelevant which P$_{O2}$ value between 100 and 1 cm/s applies. If we consider the (purple) line for P$_{O2}$ = 0.2 cm/s, i.e., the value we observe for a cholesterol concentration of 45% as it occurs in the red cell membrane (Figs. 7 and 8), we can conclude that with this P value a) we reach by far full equilibration of the red cell with the alveolar O$_2$ partial pressure within the resting capillary transit time of 0.7 s, and b) even within the minimal capillary transit time seen under maximal exercise of 0.25 s [26], equilibration is still reached by about 95%. Thus, a P$_{O2}$ of 0.2 cm/s guarantees a near complete equilibration under all physiological conditions. All curves for P$_{O2}$ ≤ 0.05 cm/s do not even achieve full equilibration at a transit time of 0.7 s and by far not at 0.25 s. The dashed lines in Fig. 9 indicate the influence of intracellular diffusion of O$_2$. The left-most dashed purple curve has been calculated for a D$_{O2}$ of $3 \cdot 10^{-4}$ cm^2/s, 38 times higher than the classical value of $0.8 \cdot 10^{-5}$ cm^2/s for the red cell interior [37–39]. This is a condition in which the complete process is no longer limited by diffusion and the kinetics of the association reaction between Hb and O$_2$ dominates. The dashed purple curve in comparison to the left-most continuous curve shows that roughly 1/2 of the normal red cell equilibration

time is due to the limited speed of intracellular O$_2$ diffusion. The second dashed curve (in red) has been calculated for an intraerythrocytic D$_{O2}$ of $5 \cdot 10^{-7}$ cm^2/s, which Richardson et al. [40] propose in analogy to their indirectly determined intraerythrocytic D$_{CO2}$. This value is about 1/16 of the "classical" value of D$_{O2}$ that has been used for the calculation of all the continuous curves in Fig. 9. The red dashed curve shows that such an extremely low intracellular O$_2$ diffusivity would result in a severe deficit in oxygenation at a transit time of 0.25 s and would neither be quite sufficient for full equilibration after 0.7 s, even at an extremely high P$_{O2}$ of 10 cm/s.

We should note that the red cell membrane is not just a cholesterol-containing lipid bilayer, but contains in addition at least 23% intrinsic protein [41]. Dotson and Pias [32] have reported that a similar protein content of the membrane reduces P$_{O2}$ to about ½, supposing of course that this protein is O$_2$-impermeable. This would lead us to a P$_{O2}$ value for the red cell membrane of 0.1 cm/s (dark-green curve in Fig. 9). It is apparent that with such a P$_{O2}$, O$_2$ uptake in the lung would be complete after 0.7 s, but would reach no more than 80% of the maximum when only a transit time of 0.25 s is available. This would constitute a serious limitation of O$_2$ uptake under conditions of heavy exercise. We know that no such limitation does in fact occur in healthy subjects. It may be speculated that here gas channels of the red cell membrane such as aquaporin-1 and Rhesus-associated glycoprotein might come into play. They are established as efficient CO$_2$ channels in this membrane [9, 10], but molecular dynamics simulations have shown—at least in the case of aquaporin-1—that the CO$_2$ channel can also act as an O$_2$ channel [42]. This could well raise P$_{O2}$ from 0.1 cm/s to 0.2 cm/s or even to the value of 0.6–0.8 cm/s proposed by Holland et al. [15], and thus guarantee a complete blood oxygenation in the lung even under conditions of heavy exercise.

Methods

Preparation of hemoglobin solutions

Red cell concentrate was obtained from the blood bank of the Medical School. Erythrocytes where washed 3× in PBS at 2000 g for 10 min at 4 °C. The cell pellet was diluted 1:6 in distilled H$_2$O and incubated for 1 h at 4 °C. To produce red cell membrane ghosts, the suspension was reconstituted to 150 mM NaCl and incubated for 30 min. Ghosts were then removed via centrifugation 2 times for 1 h at 16,000 g at 4 °C and the supernatant was decanted. The final supernatant was then concentrated in an Amicon system (Merck Amicon, Fisher Scientific, Germany) to a hemoglobin concentration of ~20 g%. For this, the solution was filled into

the Amicon chamber equipped with a 10 kDa cutoff filter using a nitrogen pressure of 5 bar. The ultrafiltration was performed under gentle stirring at 4 °C. Hemoglobin concentration was determined with Drabkin's solution.

Preparation of hemoglobin-loaded liposomes

Liposomes were prepared by standard methods [2]. Briefly, phospholipids L-α-phosphatidylcholine (PC; chicken egg, mixture of different fatty acid chain lengths with C16 and C18 dominating; Avanti Polar Lipids, Alabaster, AL, USA; product number 840051) and L-α-phosphatidylethanolamine (PE; chicken egg, mixture of different fatty acid chain lengths with C16 and C18 dominating; Avanti Polar Lipids, Alabaster, AL, USA; product number 840021) and cholesterol ($\geq 99\%$, Sigma Grade; Sigma-Aldrich) dissolved in chloroform were mixed at the desired molar ratios (PC:PE 8:2 and variable amounts of cholesterol). The lipid mixture was dried to form a smooth lipid film on the inside of a small glass vial, followed by high-vacuum drying for ≥ 3 h. The lipid film was hydrated to a concentration of 3 mg/ml in a phosphate buffer (83 mM NaCl, 40 mM Na_2HPO_4, 9.4 mM NaH_2PO_4) containing 10 g% hemoglobin (6.2 • 10^{-3} M heme), and the detergent n-octyl-β-d-glucopyranoside (β-OG; Avanti Polar Lipids, Alabaster, AL, USA) was added to a concentration of 4% (w/v). The resulting mixture was incubated with intermittent agitation for 1 h at room temperature, loaded into dialysis tubing (Spectra/Por; Spectrum Labs, Rancho Dominguez, CA, USA) with a molecular cutoff of 3500 Da and dialyzed against 200 volumes of phosphate buffer for 24 h at room temperature. Buffer was exchanged 3 times during this period. The mixture was then centrifuged at 10,000 g for 10 min and the resulting supernatant was extruded through track-etched filters of decreasing pore size, and in the final step, extruded 15 times through a 0.1 µm track-etched filter (Nucleopore; Whatman, Maidstone, UK). Extravesicular material was removed on a Superdex 200 column (GE Healthcare, Little Chalfont, UK) using the above phosphate buffer. Liposomes were stored at 4 °C.

Characterization of liposomes

Transmission electron microscopy (TEM)

Liposomes were pelleted and resuspended in a tenfold volume of fixation buffer (150 mM HEPES, pH 7.35, containing 1.5% formaldehyde and 1.5% glutaraldehyde) for 30 min at RT and overnight at 4 °C. Liposomes were postfixed in 1% osmium tetroxide 2 h at RT and 4% uranyl acetate at 4 °C overnight. After dehydration in acetone, samples were embedded in EPON. 50-nm-thick sections were post-stained with 4% uranyl acetate and lead citrate [14] and observed in a Morgagni TEM (FEI), operated in the bright field mode.

Images were recorded at 80 kV using a 2 K side mounted Veleta CCD camera, binned to 1 K. The number of unilamellar vs. bilamellar liposomes in liposomes without cholesterol was determined by inspection of a total of 793 liposomes. 12% were found to possess two rather than one membrane. Liposomes with cholesterol exhibited unilamellar liposomes only.

Determination of vesicle size by dynamic light scattering (DLS)

DLS studies were performed using a Viscotek 802 instrument (Viscotek Corporation) equipped with a single mode fiber optics and a 50 mW diode laser ($\lambda = 832$ nm) at 20 °C. The vesicle suspension was suitably diluted in a phosphate buffer as described above. Prior to dilution, the buffer was filtered through a syringe filter (Minisart®) with a pore size of 0.2 µm (Sartorius, Germany). The measurement yielded the average radius of the liposomes and their size distribution.

Cholesterol content of liposomal membranes

This was estimated from the ratio of cholesterol concentration vs. phosphatidylcholine concentration in the membrane. Cholesterol was determined using the Amplex Red Cholesterol Assay Kit (Invitrogen). Choline was determined with the Phosphatidylcholine Assay Kit (Sigma Aldrich). Fluorescence intensities were measured in a FLUOstar Optima microplate reader (BMG Labtech) and converted to molar concentrations using calibration curves. The experimental ratios of the two molar concentrations were compared with the ratios expected from the molar ratios of the two lipids in the original lipid mixture.

Stopped-flow experiments

Stopped-flow experiments were carried out in a Hi-tech Scientific SF-61 DX2 double mixing stopped-flow system from TgK Scientific Limited (Bradford-on-Avon, United Kingdom; 20 ml cuvette volume, dead time 1 ms). Syringes and mixing chamber were kept at 7 °, 25 ° or 35 °C, respectively. The hemoglobin absorbance of vesicle suspensions oxygenated in air was measured at a wavelength exhibiting a large absorbance difference between oxy- and deoyhemoglobin (436 nm). In the case of hemoglobin solutions, a higher hemoglobin concentration was used compared to the average Hb concentration of the liposome suspension, and absorbance was, therefore, recorded at a wavelength somewhat less sensitive to the absolute specific absorbances of oxy- and deoxy-Hb as well as the difference between them (470 nm). While the intravesicular Hb concentration was ~ 6.2 mM, the average Hb concentration of vesicle suspensions was

about 0.005 mM. Thus, the volume fraction of vesicles in the suspensions was of the order of 0.08 vols %. In contrast to the low Hb concentration of liposome suspensions, free hemoglobin solutions had a higher concentration of 0.077 mM, which served to prevent dissociation of Hb tetramers into dimers. One syringe of the stopped-flow apparatus contained either a suspension of Hb-loaded vesicles in the above phosphate buffer or a free Hb solution in the same buffer. In both cases, hemoglobin was fully oxygenated by equilibration in air. The other syringe contained a solution of 50 mM sodium dithionite with 40 mM Na_2HPO_4, 9.4 mM NaH_2PO_4 and 8 mM NaCl that had been prepared under anaerobic conditions and adjusted to pH 7.4, similar to the dithionite solutions used by previous investigators of the deoxygenation kinetics of hemoglobin or red cells [15, 16]. Upon mixing, all available dissolved extravesicular O₂ is consumed by dithionite extremely rapidly within the dead time of the stopped-flow apparatus (ca. 1 ms) [43, 44]. We have shown this by supplementing the equation system given below by an equation describing the kinetics of O₂ consumption by dithionite and using the kinetic constant reported by Creutz and Sutin [44]. The calculation shows in addition that the kinetics of hemoglobin deoxygenation observed after the stop is not noticeably affected by the speed of the dithionite reaction. In this latter phase after the stop, the O₂ diffuses out of the vesicles, thereby crossing the liposome membranes, into the surrounding dithionite solution, which immediately also absorbs this oxygen. Thus, O₂ partial pressure in the extravesicular space is kept zero at all times [15]. The kinetics of deoxygenation of the intravesicular hemoglobin was followed by recording the absorbance at the wavelength given above. The procedure was identical for free hemoglobin solutions, except for a different wavelength being used, as stated above, to limit the size of the absorbance signal. Using the software implemented in the stopped-flow apparatus, we usually were able to fit the records from experiments with free Hb to a first-order exponential with $R^2 > 0.999$, while the experiments with liposomes were fitted with the same quality to a second-order exponential. These exponentials provided excellent empirical descriptions of the experimental records that could be used to determine the half-times of the kinetics as shown in Fig. 4. In the case of the hemoglobin solution, the fitted first-order exponential of the form Absorbance signal $= A e^{(-k_{obs} \cdot t)}$ directly provides the rate constant of oxyhemoglobin dissociation k_d as given by the value of k_{obs} in the exponent. A in this term is the initial value of the signal at $t = 0$.

Theory of O₂ release by liposomes and calculation of O₂ permeabilities

The stopped-flow experiment starts with fully oxygenated hemoglobin (Hb) inside the liposomes (O₂ partial pressure

pO₂ = that of air) and dithionite outside the vesicles, which maintains pO₂ = 0 outside throughout the experiment. It ends when all Hb inside the vesicles is fully deoxygenated. The kinetics of this process is determined by (a) the kinetics of dissociation of Hb and O₂ within the vesicle, and (b) the diffusion of O₂ across the vesicle membrane as governed by the membrane O₂ permeability P_{O2}.

The kinetics of the reactions of oxygen and hemoglobin inside the vesicle are described by

$$\frac{\partial [O_2]_i}{\partial t} = k_d \cdot [HbO_2] - k_a \cdot [Hb] \cdot [O_2]_i, \text{and} \tag{1}$$

$$\frac{\partial [HbO_2]}{\partial t} = -k_d \cdot [HbO_2] + k_a \cdot [Hb] \cdot [O_2]_i, \tag{2}$$

where $[O_2]_i$ is the intraliposomal concentration of dissolved oxygen, and $[HbO_2]$ and $[Hb]$ are the concentrations of oxygenated and deoxygenated Hb, respectively. k_a is he association kinetic constant, and k_d is the dissociation kinetic constant.

Only dissolved oxygen is able to diffuse across the vesicle membrane and the resulting change in intravesicular oxygen concentration is described by

$$\frac{\partial [O_2]_i}{\partial t} = P_{O2} \cdot \frac{a}{v} \cdot ([O_2]_e - [O_2]_i), \tag{3}$$

where P_{O2} is the oxygen permeability of the membrane, a is the surface area of the liposomes and v is the intravesicular volume. $[O_2]_e$ is the extravesicular O₂ concentration = 0.

The right hand sides of Eqs. 1 and 3 can be added to give Eq. 4 that describes the actual change of intravesicular O₂ concentration per time $\frac{\partial [O_2]_i}{\partial t}$:

$$\frac{\partial [O_2]_i}{\partial t} = k_d \cdot [HbO_2] - k_a \cdot [Hb] \cdot [O_2]_i + P_{O2} \cdot \frac{a}{v} \cdot ([O_2]_e - [O_2]_i) \tag{4}$$

Equations 2 and 4 were then integrated numerically using MATLAB 2020a. P_{O2} was varied until the calculated kinetics exhibited a half-time identical to that of the experimental stopped-flow kinetics as shown in Fig. 3. When the external radius of the liposome is 50 nm and the thickness of the membrane is assumed to be 5 nm, the radius of the intravesicular volume containing the hemoglobin is 45 nm. a is then defined as the external surface of a sphere of 45 nm diameter, v is defined as the intravesicular volume of such a sphere. The membrane of a finite thickness is then replaced in this model by a surface of the area a and the O₂ permeability P_{O2}. This simplified model requires short computation times, but a) ignores the finite thickness of the membrane, and b) assumes a stirred intravesicular volume with the absence of any concentration gradients.

Nevertheless, as discussed below, it generates quite correct results, which deviate from those of a more realistic model only very slightly.

We have also used a more complex model, which a) considers the actual thickness of the membrane, and b) considers the simultaneous reaction and diffusion processes in the vesicle interior. For this purpose, the above equations were expanded to a more complex model as follows:

The chemical reactions were again described by Eqs. 1 and 2, and, following Crank's [25] treatment, the diffusion of O_2 and HbO_2 inside the vesicle was described by

$$\frac{\partial [O_2]}{\partial t} = D_{O_2} \cdot \frac{1}{r} \cdot \frac{\partial}{\partial r}\left(r^2 \cdot \frac{\partial [O_2]}{\partial r}\right) = D_{O_2} \cdot \left(\frac{\partial^2 [O_2]}{\partial r^2} + \frac{2}{r} \cdot \frac{\partial [O_2]}{\partial r}\right) \tag{5}$$

$$\frac{\partial [HbO_2]}{\partial t} = D_{Hb} \cdot \left(\frac{\partial^2 [HbO_2]}{\partial r^2} + \frac{2}{r} \cdot \frac{\partial [HbO_2]}{\partial r}\right) \tag{6}$$

Again, the right hand sides of Eqs. 1 and 5 as well as those of Eqs. 2 and 6 are added to describe the combined contributions of intravesicular reaction and diffusion. These equations were solved by Crank's finite difference method employing MATLAB. The entire sphere of radius 50 nm is divided into 1-nm-thick segments, within which reaction occurs and between which diffusion occurs. The complete sphere includes a membrane of an assumed 5 nm thickness, i.e., 5 segments. Integration is performed over the complete radius of 50 nm. However, the five layers representing the membrane lack hemoglobin, and thus, Eqs. 1, 2 and 6 are omitted. The problem of the transition between the membrane and the water phase was handled as described by Crank [24] in Eq. 8.45 on p. 150. The five membrane layers are given a homogeneous membrane $D_{O2,M}$ that replaces D_{O2} in the above equations and together with the 5 nm thickness defines membrane $P_{O2} = D_{O2,M}/5$ nm. This $D_{O2,M}$ is varied until it gives calculated half-times which agree with the experimental half-times of the stopped-flow records.

Sensitivity of calculation for thickness of the membrane

In terms of the membrane barrier, the assumed membrane thickness is irrelevant, because the lower thickness of a thinner membrane will be compensated by a lower $D_{O2,M}$, giving an identical P_{O2}. However, in the complex model the membrane thickness is relevant in terms of the intravesicular volume. We have tested this effect using a modification of the described calculation by assuming a 4-nm-thick membrane, which is represented by four 1-nm-thick layers (complemented by 46 layers representing the vesicle interior). Of course, the values $D_{O2,M}$ in these four 1-nm-thick membrane layers then turn out to be only about 4/5 of those in the five

membrane layers. Evidently, the intravesicular volume is somewhat larger in this modified model. However, effects of the five- vs. four-layer model on the calculations are small. Between P_{O2} values of 0.03 and 0.2 cm/s, the deviations in calculated $t_{1/2}$ are between < 1 and 2%. From this, we conclude that an uncertainty in the actual membrane thickness and the associated alteration of intravesicular water volume have no substantial consequence for the calculated $t_{1/2}$ and thus for the estimated P_{O2}.

Role of intravesicular diffusion

To make an approximate comparison possible between the simple model of Eq. 4, which assumes a stirred intravesicular volume, and the complex model, which takes intravesicular diffusion into account, we use the following approach. The complex model is equipped with a 1-nm-thick membrane, i.e., one 1-nm-thick layer for the membrane and 49 layers for the vesicle interior. This geometrical situation comes close to the situation in the simple model of a vesicle of 50 nm radius, in which the membrane has in effect no thickness. Thus, a difference between the two modes of calculation can approximately be attributed to the effect of intravesicular diffusion. Between P_{O2} values of 0.03 and 0.2 cm/s, the deviations in calculated $t_{1/2}$ are all $\leq 1\%$. This result is unaltered, when we use in the complex model a membrane thickness of 0.5 nm instead of 1 nm. This shows that intravesicular diffusion contributes entirely insignificantly to the deoxygenation kinetics of the liposomes.

Overall, the computations with the simple model provide a very good approximation of the result obtained with the complex model. This allowed us to first apply the experimental results to model one, and then use the result to obtain with little or no fitting the final result on the basis of the complex model with 5 membrane layers. Deviations between the $t_{1/2}$ values from the two modes of computation were no greater than 1–3%.

Boundary conditions and constants

The initial oxygen partial pressure pO_2 within the vesicle was that of air, about 150 mmHg, and the intravesicular hemoglobin initially was maximally loaded with O_2. The extravesicular pO_2 was 0 mmHg at all times. The time intervals used in the numerical integration of the complex model must be sufficiently small to ensure stable numerical integration; usually a time interval of 0.1 ns was used, which made these computations rather time-consuming. The constants employed in the calculations were, at the temperatures 7 °, 25 ° and 35 °C, for D_{O2}: $1.1 \cdot 10^{-5}$, $1.8 \cdot 10^{-5}$ and $2.4 \cdot 10^{-5}$ cm^2/s ([17], corrected for intravesicular Hb after [45]), for solubility α_{O2}: $2.33 \cdot 10^{-3}$, $1.60 \cdot 10^{-3}$ and $1.41 \cdot 10^{-3}$ mmol/l/mmHg [46], for oxygen affinity p_{50} in

the absence of 2,3-BPG: 1.70, 6.31 and 12.6 mmHg [16], for D$_{Hb}$: 34 • 10^{-8}, 51 • 10^{-8} and 64 • 10^{-8} cm^2/s ([47], corrected for temperatures), respectively. The equilibrium constant K_d describing the equilibrium of Hb, O$_2$ and HbO$_2$ was obtained as $\alpha_{O2} • p_{50}$. The rate constants k_d describing the dissociation of O$_2$ from HbO$_2$ used in the calculations were obtained from the present stopped-flow measurements mixing oxyhemoglobin solutions with dithionite solutions and had the values 5.62, 56.8 and 175 s^{-1}. The rate constants k_a of the association of Hb and O$_2$ were obtained as the ratios of k_d over the equilibrium constant K_d.

Declarations

References

1. Arias-Hidalgo M, Al-Samir S, Gros G, Endeward V (2018) Cholesterol is the main regulator of the carbon dioxide permeability of biological membranes. Am J Physiol-Cell Physiol 315:C137–C140. https://doi.org/10.1152/ajpcell.00139.2018

2. Itel F, Al-Samir S, Öberg F et al (2012) CO2 permeability of cell membranes is regulated by membrane cholesterol and protein gas channels. FASEB J 26:5182–5191. https://doi.org/10.1096/fj.12-209916

3. Tsiavaliaris G, Itel F, Hedfalk K et al (2015) Low CO2 permeability of cholesterol-containing liposomes detected by stopped-flow fluorescence spectroscopy. FASEB J 29:1780–1793. https://doi.org/10.1096/fj.14-263988

4. Kai L, Kaldenhoff R (2014) A refined model of water and CO2 membrane diffusion: Effects and contribution of sterols and proteins. Sci Rep 4:1–6. https://doi.org/10.1038/srep06665

5. Blosser MC, So J, Madani MS, Malmstadt N (2020) Effect of cholesterol on permeability of carbon dioxide across lipid membranes. bioRxiv. https://doi.org/10.1101/2020.11.16.384958

6. Blanco-Ameijeiras S, Stoll HM, Zhang H, Hopkinson BM (2020) Influence of temperature and CO2 On plasma-membrane permeability to CO2 and HCO3− in the marine haptophytes *Emiliania huxleyi* and *Calcidiscus leptoporus* (Prymnesiophyceae). J Phycol 56:1283–1294. https://doi.org/10.1111/jpy.13017

7. Uehlein N, Lovisolo C, Siefritz F, Kaldenhoff R (2003) The tobacco aquaporin NtAQP1 is a membrane CO2 pore with physiological functions. Nature 425:734–737. https://doi.org/10.1038/nature02027

8. Nakhoul NL, Davis BA, Romero M, Boron W (1998) Effect of expressing the water channel aquaporin-1 on the CO2 permeability of Xenopus oocytes. Am J Physiol 274:C543–C548. https://doi.org/10.1152/ajpcell.1998.274.2.c297

9. Endeward V, Musa-Aziz R, Cooper GJ et al (2006) Evidence that aquaporin 1 is a major pathway for CO2 transport across the human erythrocyte membrane. FASEB J 20:1974–1981. https://doi.org/10.1096/fj.04-3300com

10. Endeward V, Cartron JP, Ripoche P, Gros G (2008) RhAG protein of the Rhesus complex is a CO2 channel in the human red cell membrane. FASEB J 22:64–73. https://doi.org/10.1096/fj.07-9097com

11. Subczynski W, Hyde J, Kusumi A (1989) Oxygen permeability of phosphatidylcholine-cholesterol membranes. Proc Natl Acad Sci USA 86:4474–4478

12. De Vos O, Venable RM, Van Hecke T et al (2018) Membrane permeability: characteristic times and lengths for oxygen and a simulation-based test of the inhomogeneous solubility-diffusion model. J Chem Theory Comput 14:3811–3824. https://doi.org/10.1021/acs.jctc.8b00115

13. Krämer A, Ghysels A, Wang E et al (2020) Membrane permeability of small molecules from unbiased molecular dynamics simulations. J Chem Phys. https://doi.org/10.1063/5.0013429

14. Möller MN, Cuevasanta FO, Lopez AC et al (2019) Diffusion and transport of reactive species across cell membranes. In: Trostchansky A, Rubbo H (eds) Bioactive lipids in health and disease, vol 1127. Adv Exp Med Biol, Springer Nature, Switzerland, pp 3–19

15. Holland RAB, Shibata H, Scheid P, Piiper J (1985) Kinetics of O2 uptake and release by red cells in stopped-flow apparatus: effects of unstirred layer. Respir Physiol 59:71–91. https://doi.org/10.1016/0034-5687(85)90020-9

16. Bauer C, Klocke RA, Kamp D, Forster RE (1973) Effect of 2,3-diphosphoglycerate and H+ on the reaction of O2 and hemoglobin. Am J Physiol 224:838–847

17. Himmelblau DM (1964) Diffusion of dissolved gases in liquids. Chem Rev 64:527–550. https://doi.org/10.1021/cr60231a002

18. Ghysels A, Krämer A, Venable RM et al (2019) Permeability of membranes in the liquid ordered and liquid disordered phases—suppl inform. Nat Commun 10:1–13. https://doi.org/10.1038/s41467-019-13432-7

19. Ghysels A, Venable R, Pastor R, Hummer G (2017) Position dependent diffusion tensors in anisotropic media from simulation: oxygeen transport in and through membranes. J Chem Theory Comput 13:2962–2976. https://doi.org/10.1021/acs.jctc.7b00039

20. Dotson RJ, Smith CR, Bueche K et al (2017) Influence of cholesterol on the oxygen permeability of membranes: insight from atomistic simulations. Biophys J 112:2336–2347. https://doi.org/10.1016/j.bpj.2017.04.046

21. Angles G, Dotson R, Bueche K, Pias SC (2017) Predicted decrease in membrane oxygen permeability with addition of cholesterol. Adv Exp Med Biol 977:9–14. https://doi.org/10.1007/978-3-319-55231-6

22. Hannesschlaeger C, Horner A, Pohl P (2019) Intrinsic membrane permeability to small molecules. Chem Rev 119:5922–5953. https://doi.org/10.1021/acs.chemrev.8b00560

23. Endeward V, Gros G (2009) Extra- and intracellular unstirred layer effects in measurements of CO2 diffusion across membranes—a novel approach applied to the mass spectrometric 18O technique for red blood cells. J Physiol 587:1153–1167. https://doi.org/10.1113/jphysiol.2008.165027

24. Landau LD, Lifschitz EM (1991) Lehrbuch der theoretischen physik. Hydrodynamik, vol VI. Akademie-Verlag, Berlin (**5. Auflage**)

25. Crank J (1975) The mathematics of diffusion, 2nd edn. Clarendon Press, Oxford

26. Wagner PD (1977) Diffusion and chemical reaction in pulmonary gas exchange. Physiol Rev 57:257–312. https://doi.org/10.1152/physrev.1977.57.2.257

27. Waisbren SJ, Geibel JP, Modlin IM, Boron WF (1994) Unusual permeability properties of gastric gland cells. Nature 368:332–335

28. Endeward V, Gros G (2005) Low carbon dioxide permeability of the apical epithelial membrane of guinea-pig colon. J Physiol 567:253–265. https://doi.org/10.1113/jphysiol.2005.085761

29. Hasselblatt P, Warth R, Schulz-Baldes A et al (2000) pH regulation in isolated in vitro perfused rat colonic crypts. Pflugers Arch Eur J Physiol 441:118–124. https://doi.org/10.1007/s004240000377

30. Hill WG, Zeidel ML (2000) Reconstituting the barrier properties of a water-tight epithelial membrane by design of leaflet-specific liposomes. J Biol Chem 275:30176–30185. https://doi.org/10.1074/jbc.M003494200

31. Endeward V, Al-Samir S, Itel F, Gros G (2014) How does carbon dioxide permeate cell membranes? A discussion of concepts, results and methods. Front Physiol. https://doi.org/10.3389/fphys.2013.00382

32. Dotson RJ, Pias SC (2018) Reduced oxygen permeability upon protein incorporation within phospholipid bilayers. Adv Exp Med Biol 1072:405–411. https://doi.org/10.1007/978-3-319-91287-5

33. Fornasier F, Souza LMP, Souza FR et al (2020) Lipophilicity of coarse-grained cholesterol models. J Chem Inf Model 60:569–577. https://doi.org/10.1021/acs.jcim.9b00830

34. De Meyer F, Smit B (2009) Effect of cholesterol on the structure of a phospholipid bilayer. Proc Natl Acad Sci U S A 106:3654–3658. https://doi.org/10.1073/pnas.0809959106

35. Needham D, Nunn RS (1990) Elastic deformation and failure of lipid bilayer membranes containing cholesterol. Biophys J 58:997–1009. https://doi.org/10.1016/S0006-3495(90)82444-9

36. Miyamoto Y, Moll W (1971) Measurements of dimensions and pathway of red cells in rapidly frozen lungs in situ. Respir Physiol 12:141–156. https://doi.org/10.1016/0034-5687(71)90047-8

37. Grote J, Thews G (1962) Die Bedingungen für die Sauerstoffversorgung des Herzmuskelgewebes. Pflugers Arch Gesamte Physiol Menschen Tiere 276:142–165. https://doi.org/10.1007/BF00363329

38. Kreuzer F, Yahr WZ (1960) Influence of red cell membrane on diffusion of oxygen. J Appl Physiol 15:1117–1122. https://doi.org/10.1152/jappl.1960.15.6.1117

39. Moll W (1969) The influence of hemoglobin diffusion on oxygen uptake and release by red cells. Resp Physiol 6:1–15. https://doi.org/10.1016/0034-5687(68)90014-5

40. Richardson SL, Hulikova A, Proven M et al (2020) Single-cell O2 exchange imaging shows that cytoplasmic diffusion is a dominant barrier to efficient gas transport in red blood cells. Proc Natl Acad Sci. https://doi.org/10.1073/pnas.1916641117

41. Dupuy AD, Engelman DM (2008) Protein area occupancy at the center of the red blood cell membrane. Proc Natl Acad Sci U S A 105:2848–2852. https://doi.org/10.1073/pnas.0712379105

42. Wang Y, Cohen J, Boron WF et al (2007) Exploring gas permeability of cellular membranes and membrane channels with molecular dynamics. J Struct Biol 157:534–544. https://doi.org/10.1016/j.jsb.2006.11.008

43. Morello JA, Craw MR, Constantine HP, Forster RE (1964) Rate of reaction of dithionite ion with oxygen in aqueous solution. J Appl Physiol 19:522–525

44. Creutz C, Sutin N (1974) Kinetics of the reactions of sodium dithionite with dioxygen and hydrogen peroxide. Inorg Chem 13:2041–2043

45. Keller KH, Friedlander SK (1966) The steady-state transport of oxygen through hemoglobin solutions. J Gen Physiol 49:663–679. https://doi.org/10.1085/jgp.49.4.663

46. Bartels H, Bücherl E, Hertz C et al (1959) Lungenfunktionsprüfungen, 1st edn. Springer, Berlin-Göttingen-Heidelberg

47. Gros G (1978) Concentration dependence of the self-diffusion of human and Lumbricus terrestris hemoglobin. Biophys J 22:453–468. https://doi.org/10.1016/S0006-3495(78)85499-X